The substrate-bound nanowires were sonicated in ethanol and deposited on oxidized degenerately doped silicon wafers or copper grids for electrical transport and TEM measurements, respectively. Electron-beam lithography was employed to define contact regions with subsequent deposition of Ti/Au electrodes, as described previously[3]. Effective mobilities were calculated according to the method of ref. 26. Additional details are provided in the Supplementary Information. The integrity of the SiO_x gate dielectric in the coaxially gated nanowire transistors was confirmed by the low, <5 pA, gate to source–drain leakage currents. The continuity of the p-Ge outer shell was verified by two-terminal resistance measurements on the shell itself.

The high-resolution TEM images were collected on a Jeol 2010F microscope, and elemental imaging and cross-sectional mapping was conducted on a VG HB603 STEM. The elemental mapping data were modelled by calculating the cross-sectional thicknesses for concentric cylinders of different composition with abrupt interfaces, taking the electron beam profile into account by convoluting with a gaussian profile of 1.6 ± 0.5 nm full-width, consistent with the known value for the instrument.

Received 5 June; accepted 24 September 2002; doi:10.1038/nature01141.

1. Sze, S. M. *Physics of Semiconductor Devices* (Wiley-Interscience, New York, 1981).
2. Lieber, C. M. The incredible shrinking circuit. *Sci. Am.* **285,** 58–64 (2001).
3. Cui, Y. & Lieber, C. M. Functional nanoscale electronic devices assembled using silicon nanowire building blocks. *Science* **291,** 851–853 (2001).
4. Duan, X. F., Huang, Y., Cui, Y., Wang, J. F. & Lieber, C. M. Indium phosphide nanowires as building blocks for nanoscale electronic and optoelectronic devices. *Nature* **409,** 66–69 (2001).
5. Cui, Y., Wei, Q. Q., Park, H. K. & Lieber, C. M. Nanowire nanosensors for highly sensitive and selective detection of biological and chemical species. *Science* **293,** 1289–1292 (2001).
6. Huang, Y. *et al.* Logic gates and computation from assembled nanowire building blocks. *Science* **294,** 1313–1317 (2001).
7. Nirmal, M. & Brus, L. Luminescence photophysics in semiconductor nanocrystals. *Acc. Chem. Res.* **32,** 407–414 (1999).
8. Bruchez, M., Moronne, M., Gin, P., Weiss, S. & Alivisatos, A. P. Semiconductor nanocrystals as fluorescent biological labels. *Science* **281,** 2013–2016 (1998).
9. Chan, W. C. W. & Nie, S. M. Quantum dot bioconjugates for ultrasensitive nonisotopic detection. *Science* **281,** 2016–2018 (1998).
10. Klimov, V. I. *et al.* Optical gain and stimulated emission in nanocrystal quantum dots. *Science* **290,** 314–317 (2000).
11. Gudiksen, M. S., Lauhon, L. J., Wang, J., Smith, D. C. & Lieber, C. M. Growth of nanowire superlattice structures for nanoscale photonics and electronics. *Nature* **415,** 617–620 (2002).
12. Bjork, M. T. *et al.* One-dimensional heterostructures in semiconductor nanowhiskers. *Appl. Phys. Lett.* **80,** 1058–1060 (2002).
13. Wu, Y. Y., Fan, R. & Yang, P. D. Block-by-block growth of single-crystalline Si/SiGe superlattice nanowires. *Nano Lett.* **2,** 83–86 (2002).
14. Jones, A. C. & O'Brien, P. *CVD of Compound Semiconductors: Precursor Synthesis, Development and Applications* (VCH, Weinheim, 1997).
15. Duan, X. F. & Lieber, C. M. General synthesis of compound semiconductor nanowires. *Adv. Mater.* **12,** 298–302 (2000).
16. Gudiksen, M. S. & Lieber, C. M. Diameter-selective synthesis of semiconductor nanowires. *J. Am. Chem. Soc.* **122,** 8801–8802 (2000).
17. Mooney, P. M. & Chu, J. O. SiGe technology: Heteroepitaxy and high-speed microelectronics. *Annu. Rev. Mater. Sci.* **30,** 335–362 (2000).
18. Cui, Y., Lauhon, L. J., Gudiksen, M. S., Wang, J. F. & Lieber, C. M. Diameter-controlled synthesis of single-crystal silicon nanowires. *Appl. Phys. Lett.* **78,** 2214–2216 (2001).
19. Briand, D., Sarret, M., Kis-Sion, K., Mohammed-Brahim, T. & Duverneuil, P. In situ doping of silicon deposited by LPCVD: pressure influence on dopant incorporation mechanisms. *Semicond. Sci. Technol.* **14,** 173–180 (1999).
20. Cheng, I. C. & Wagner, S. Hole and electron field-effect mobilities in nanocrystalline silicon deposited at 150 degrees C. *Appl. Phys. Lett.* **80,** 440–442 (2002).
21. Klaassen, D. B. M. A unified mobility model for device simulation. 1. Model-equations and concentration-dependence. *Solid-State Electron.* **35,** 953–959 (1992).
22. Hull, R.Bean, J. C. (ed.) *Germanium Silicon: Physics and Materials* (Academic, San Diego, 1999).
23. Grutzmacher, D. A. *et al.* Ge segregation in SiGe/Si heterostructures and its dependence on deposition technique and growth atmosphere. *Appl. Phys. Lett.* **63,** 2531–2533 (1993).
24. Wind, S. J., Appenzeller, J., Martel, R., Derycke, V. & Avouris, P. Vertical scaling of carbon nanotube field-effect transistors using top gate electrodes. *Appl. Phys. Lett.* **80,** 3817–3819 (2002).
25. Solomon, P. M. Device innovation and material challenges at the limits of CMOS technology. *Annu. Rev. Mater. Sci.* **30,** 681–697 (2000).
26. Martel, R., Schmidt, T., Shea, H. R., Hertel, T. & Avouris, P. Single- and multi-wall carbon nanotube field-effect transistors. *Appl. Phys. Lett.* **73,** 2447–2449 (1998).
27. Gibson, J. M., Lanzerotti, M. Y. & Elser, V. Plan-view transmission electron diffraction measurement of roughness at buried Si/SiO2 interfaces. *Appl. Phys. Lett.* **55,** 1394–1396 (1989).

Supplementary Information accompanies the paper on *Nature*'s website (http://www.nature.com/nature).

Acknowledgements We thank A. J. Garratt-Reed for assistance with TEM imaging and analysis. M.S.G. thanks the NSF for predoctoral fellowship support. C.M.L. acknowledges support of this work by the Office of Naval Research and Defense Advanced Research Projects Agency.

Competing interests statement The authors declare that they have no competing financial interests.

Correspondence and requests for materials should be addressed to C.M.L. (e-mail: cml@cmliris.harvard.edu).

The amount of carbon released from peat and forest fires in Indonesia during 1997

Susan E. Page*, Florian Siegert†‡, John O. Rieley§, Hans-Dieter V. Boehm‡, Adi Jaya‖ & Suwido Limin‖

** Department of Geography, University of Leicester, Leicester LE1 7RH, UK*
† Ludwigs-Maximilians-Universität München, Biology Department II, Luisenstrasse 14, D-80333 München, Germany, and Remote Sensing Solutions GmbH, Woerthstrasse 49, D-81667 München, Germany
‡ Kalteng Consultants, Kirchstockacher Weg, 81663 München, Germany
§ School of Geography, University of Nottingham, Nottingham NG7 2RD, UK
‖ Centre for International Co-operation in Management of Tropical Peatland, Faculty of Agriculture, University of Palangka Raya, Palangka Raya 73112, Indonesia

Tropical peatlands are one of the largest near-surface reserves of terrestrial organic carbon, and hence their stability has important implications for climate change[1–3]. In their natural state, lowland tropical peatlands support a luxuriant growth of peat swamp forest overlying peat deposits up to 20 metres thick[4,5]. Persistent environmental change—in particular, drainage and forest clearing—threatens their stability[2], and makes them susceptible to fire[6]. This was demonstrated by the occurrence of widespread fires throughout the forested peatlands of Indonesia[7–10] during the 1997 El Niño event. Here, using satellite images of a 2.5 million hectare study area in Central Kalimantan, Borneo, from before and after the 1997 fires, we calculate that 32% (0.79 Mha) of the area had burned, of which peatland accounted for 91.5% (0.73 Mha). Using ground measurements of the burn depth of peat, we estimate that 0.19–0.23 gigatonnes (Gt) of carbon were released to the atmosphere through peat combustion, with a further 0.05 Gt released from burning of the overlying vegetation. Extrapolating these estimates to Indonesia as a whole, we estimate that between 0.81 and 2.57 Gt of carbon were released to the atmosphere in 1997 as a result of burning peat and vegetation in Indonesia. This is equivalent to 13–40% of the mean annual global carbon emissions from fossil fuels, and contributed greatly to the largest annual increase in atmospheric CO_2 concentration detected since records began in 1957 (ref. 1).

In Indonesia, peatland fires are mostly anthropogenic, started by local (indigenous) and immigrant farmers as part of small-scale land clearance activities, and also, on a much larger scale, by private companies and government agencies as the principal tool for clearing forest, before establishing crops[9,11,12]. During the abnormally long, El Niño dry season of 1997, many of these 'managed' fires spread out of control, consuming not only the surface vegetation but also the underlying peat and tree roots, contributing to the dense haze that blanketed a large part of Southeast Asia and causing both severe deterioration in air quality and health problems[9,11].

In order to investigate the role of peatland in the release of carbon during the 1997 fires in Indonesia, we focused on 2.5 million hectares of landscape in Central Kalimantan within a single Landsat TM (thematic mapper) image. We determined land cover types and the total area of peatland. The latter includes natural and semi-natural vegetation (peat swamp forest, PSF) and land converted to various other types of use (such as the ill-fated Mega Rice Project (MRP) that was promoted by the Indonesian government from 1995 to 1999 (Fig. 1a)). By combining peat thickness, pre-fire land cover and burnt area data we were able to estimate the amount of carbon released from peatland during the fires. Our objectives were to: (1) provide accurate information on the location and extent of

fires, (2) compare the extent of fire damage between pristine and degraded peatland, and (3) estimate the scale of carbon emissions arising from the fires. We used this information to extrapolate the probable magnitude of carbon emissions from the total peatland area in Indonesia affected by the 1997 fires.

Using Landsat TM/ETM (enhanced thematic mapper) imagery (Fig. 1b) and field checking (ground-truthing), we determined that in the 2.5-Mha study area, peatland covers 86.4% of the landscape and, before the fires (Fig. 1d, Table 1), 64.3% (1,602,413 ha) of the total area was covered by dense forest (classes 1–6) with an additional 10.3% (257,713 ha) of forest mosaics (10–40% forest cover and >10% canopy cover[13]). Land used for agriculture and plantations occupied 14.0%, while 8.3% was bushland (fallow land with some vegetation regrowth after land clearance or fire damage) and 3.0% was swampy grassland. The land cover types on peatland were PSF (pristine, logged over and fragmented), forest mosaics, agricultural land and bushland. PSF occupied 85.3% (1,366,754 ha) of the forested area, of which 15.9% was pristine, 78.3% logged over and 5.8% fragmented (40–70% forest cover and >10% canopy[13]).

Optical satellite systems were severely hampered owing to

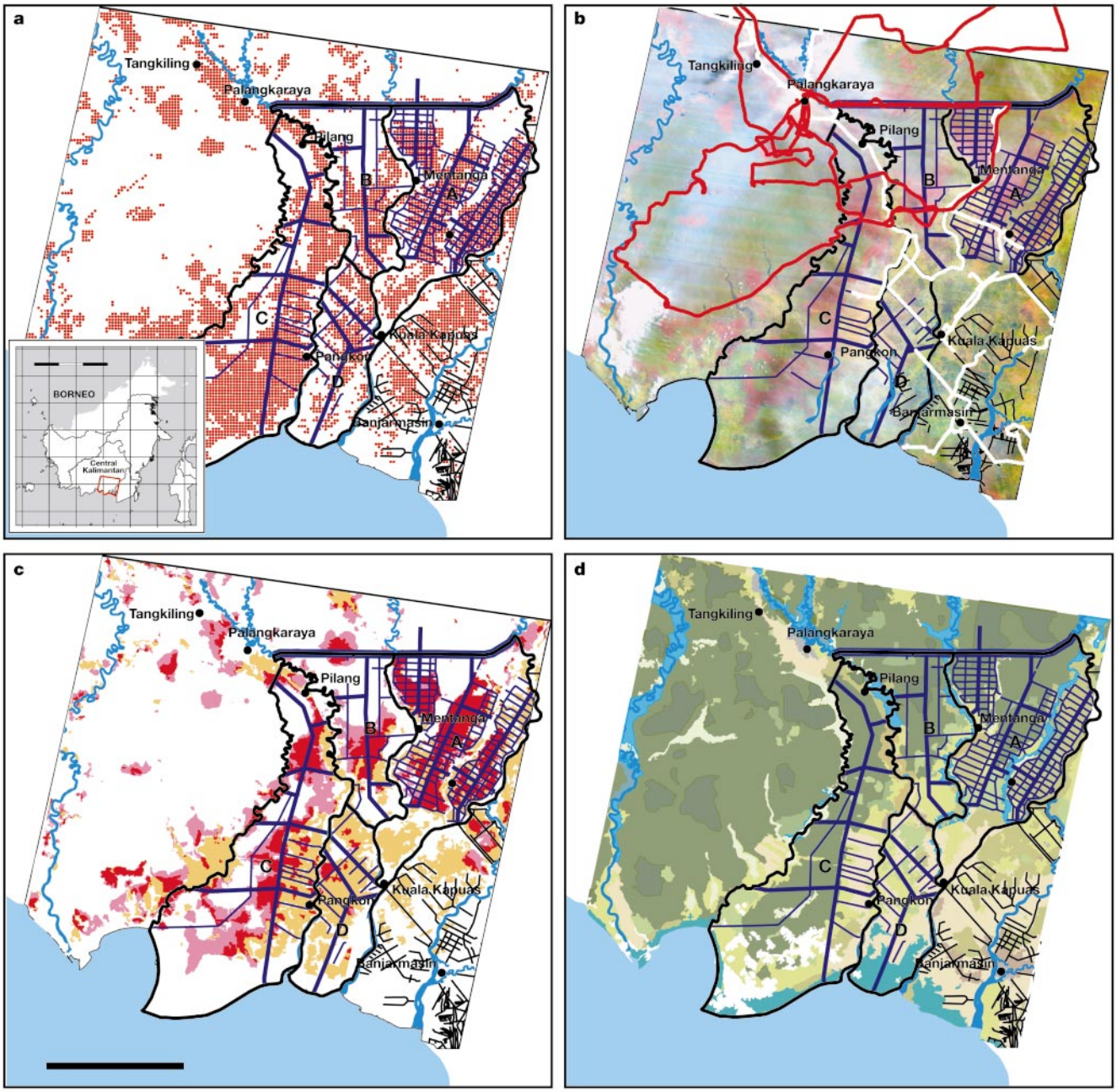

Figure 1 Study site in Central Kalimantan, Borneo, Indonesia (location see inset; bar 600 km). **a**, The four blocks of the 1-Mha MRP area (A–D) are indicated by black outlines; irrigation canals constructed between 1996 and 1997 are indicated in blue; superimposed (red dots) are NOAA AVHRR hotspots detected between June and December 1997. **b**, Post-fire Landsat TM 5 image 118-62, 29 March 1998; burn scars are visible in shades of red (RGB: TM 5 bands 5, 4, 3); superimposed are GPS-recorded ground (white) and aerial (red) surveys. **c**, Burned area derived from analysis of post-fire Landsat TM 5 and multitemporal ERS SAR images (bar 50 km); burnt areas detected by both Landsat and ERS are indicated in red; burnt areas detected only by Landsat are shown in purple; burnt areas detected only by ERS SAR and undetectable by Landsat TM 5, owing to plant regrowth are shown in orange. **d**, Land cover map derived from pre-fire Landsat TM 5 image 118-62, 29 May 1997 (dark green, low pole peat swamp forest (PSF); green, tall PSF; beige, agriculture and fallow land; bright green, fragmented PSF and PSF mosaics; brown green, grass and bushland; blue green, mangrove forests; light blue green, pristine swamp forest (periodically inundated); pale green, dry and swampy grasslands; white, clouds; blue, rivers).

Table 1 **Land cover in Central Kalimantan and the effects of the 1997 fires**

	Total study area		Former MRP		Block C of MRP	
Land cover types*	Total area (10^3 ha)	Damage in class (%)	Total area (10^3 ha)	Damage in class (%)	Total area (10^3 ha)	Damage in class (%)
1, Pristine PSF	217.1	4.5	19.4	14.1	1.9	99.3
2, Logged over PSF	1,070.7	29.2	373.6	56.8	179.7	56.1
3, Fragmented PSF	79.0	70.0	59.3	73.9	18.5	45.0
4, Riverine swamp forest	16.8	7.1	5.2	13.2	2.2	9.9
5, Fragmented riverine swamp forest	130.5	15.7	48.6	17.2	4.9	4.0
6, Mangrove forest	88.4	14.6	56.0	22.0	23.4	0
7, Forest mosaics	257.7	54.1	158.4	54.1	73.8	45.6
8, Bushland	207.9	45.2	111.3	55.3	17.4	46.4
9, Swampy grasslands	75.8	41.0	19.7	57.3	14.4	68.2
10, Agricultural land	321.0	36.9	132.9	51.1	46.4	68.6
11, Plantations	26.8	6.3	4.3	11.0	1.3	6.1
Total forest	1,602.4	25.7	562.0	49.8	230.5	48.3
Non-forest	889.2	43.2	426.6	53.2	153.3	54.5
Total PSF	1,366.8	27.6	452.3	57.2	200.1	55.5
Total peatland	2,153.3	33.9	854.8	55.5	337.6	54.7
Non-peatland	338.3	19.9	133.8	24.7	46.2	22.4
Total area	2,491.6	32.0	988.6	51.3	383.8	50.8

MRP, Mega Rice Project; PSF, peat swamp forest.
*Initial numbers represent classes: see text.

residual haze after the fires and by frequent cloud cover in the aftermath of the El Niño, so we used multitemporal, synthetic aperture radar (SAR) in addition to Landsat TM/ETM imagery to determine the extent of the burnt areas. The combined evaluation shows that 32.0% (796,907 ha) of the investigation area was burned, 91.5% (729,500 ha) of which was peatland. Of this fire-damaged peatland area, 47.4% (377,814 ha) was PSF (pristine, logged and fragmented) and the rest was degraded and deforested peatland (Fig. 1c). Only 4.5% of the pristine PSF was lost, while 29.2% of logged over and 70.0% of fragmented PSF were destroyed by fire. Severe damage also occurred to forest mosaics (54.1%), bushland (45.2%) and agricultural land (36.9%). The fire-damaged peatland represents 29.3% of the study area and 33.9% of the peatland within it.

We also compared the areas of each land cover type burned within and outside the boundary of the MRP in order to determine the effect of a major land use change on the incidence of fire. The most severely fire-damaged land cover types within the MRP were logged over and fragmented PSF and forest mosaics, of which 56.8%, 73.9% and 54.1% burned, respectively (Table 1). By the start of the fires in 1997, only a small area of pristine PSF remained within the MRP area and 14.1% of this burned, compared with only 3.6% of the much larger area of PSF outside the MRP. Clearly, forest clearance and peat drainage increased the likelihood of fire, because 51.3% of the MRP area burned compared to only 19.3% outside the MRP. This is confirmed by the spatial pattern of fire occurrences (NOAA AVHRR hotspots in Fig. 1a; see methods) and burn scars within the MRP. These show that most damage occurred adjacent to the recently excavated drainage and irrigation channels along which people gained access (Fig. 1a, c). In comparison, the large area of relatively undisturbed, undrained PSF, outside the MRP to the west of the River Sebangau (to the left in Fig. 1a, c), had only a few scattered fire scars, probably associated with illegal logging.

To obtain more accurate information on the amount of carbon stored in this peatland landscape, and to determine how much of this was burned away in the fires, we carried out a detailed study of peat thickness and surface topography within Block C (383,800 ha), the most westerly part of the MRP between the Kahayan and Sebangau rivers (Fig. 1a). We found that this peat-covered landscape is dome-shaped, with a maximum thickness of 8 m. Analysis of 126 field drillings gave a mean peat thickness in Block C of 4.4 ± 0.2 m, equating to a mean volume of peat of $(14.9 \pm 0.3) \times 10^9$ m^3. In order to compensate for those areas where the peat was shallow or non-existent (that is, <0.5 m surface organic layer; for example, close to the major rivers and near to the coast), we applied a Geographical Information System (GIS) inverse distance related (IDW) interpolation model to this entire interfluvial peatland catchment to ensure we did not over-estimate the mean peat thickness. This provided a reduced estimate of 2.3 m for average peat thickness throughout Block C, with a mean volume of 7.8×10^9 m^3. It is very difficult to determine the amount of peat destroyed by the fires, because few measurements were made of this

Table 2 **Effects of the 1997 fires on peat and carbon stores**

	Block C of MRP, 383,800 ha	Entire MRP, 988,568 ha	Study area, 2,491,619 ha	Extrapolated values for whole of Indonesia, 190,400,000 ha		
Peatland area (ha)	337,632	854,809	2,153,304	20,072,825 (ref. 4)		
Peat volume* (10^9 m^3)	7.8–14.9	19.7–37.6	49.5–94.7	461.7–883.2		
Carbon store*,† (Gt)	0.44–0.85	1.12–2.14	2.82–5.40	26.32–50.34		
				Lower estimate	Intermediate estimate	Upper estimate
Area of fire-damaged peatland (ha)	184,564 (48.1%)	474,009 (48.0%)	729,500 (29.3%)	1,450,000¶	2,441,000‖	6,804,688§
Per cent of peatland area damaged	54.7%	55.5%	33.9%	7.2%	12.1%	33.9%§
Peat volume loss‡ (10^9 m^3)	0.85–1.03	2.18–2.66	3.36–4.09	6.67–8.12	11.23–13.67	31.30–38.30
Peat carbon loss to atmosphere‡ (Gt)	0.05–0.06	0.12–0.15	0.19–0.23	0.38–0.46	0.64–0.78	1.78–2.17
Per cent peat carbon loss from store‡	5.9–13.6%	5.6–13.4%	3.5–8.2%	0.8–1.8%	1.3–3.0%	3.5–8.2%
Biomass carbon loss# (Gt)	0.01	0.03	0.05	0.10	0.17	0.40
Total carbon loss (Gt)	0.06–0.07	0.15–0.18	0.24–0.28	0.48–0.56	0.81–0.95	2.18–2.57

*Range derived from the IDW interpolation model, average peat thickness of 2.3 m; and 4.4 m from 126 field drillings.
†Based on a peat bulk density of 0.1 g cm^{-3}, and peat carbon content of 57% (0.57)[18].
‡Using 0.51 m for the estimated average depth by which peat burned down in the 1997 fires.
§Derived from the total area of peatland in Indonesia (20,072,825 ha; ref. 4) and an assumption, based on this study, that on 33.9% of this area an average of 0.51 ± 0.05 m of peat burned away.
‖Based on the sum of: 730,000 ha for our 2.5-Mha study area, 700,000 ha for the rest of Central and West Kalimantan (derived from our own satellite imagery and land cover maps), 311,000 ha for East Kalimantan[2], 400,000 ha for West Papua[9] and 300,000 ha for Sumatra[9]. The data for West Papua are uncorroborated, and those for Sumatra are probably gross underestimates.
¶Ref. 9.
#Based on vegetation biomass[15] carbon content of 250 t C ha^{-1}, 50% of which was liberated in the fires.

damage at the time and the evidence has now been covered over by regenerating vegetation. We obtained some data, however, on the thickness of peat burned away by measuring from the former peat surface, determined by observing adjacent, unburnt PSF, to the post-fire level. These varied between 25 and 85 cm with an average of 51 ± 5 cm (95% confidence limit). We estimated the loss of carbon to the atmosphere as a result of fires burning in the peat within Block C, and then extrapolated the probable carbon losses to the atmosphere from the whole of the MRP area, our study area of 2.5 Mha and the total peatland area of Indonesia in 1997[9,10,14] (Table 2).

According to our data, 0.19–0.23 Gt C (3.5–8.2%) of the total carbon stored in the 2.5-Mha study area was released in the 1997 fires while, in the MRP, 0.12–0.15 Gt C (5.6–13.4%) of the peat carbon was transferred to the atmosphere. These values do not take into account the amount of carbon lost in biomass burning but, on the basis of a carbon content for pristine PSF[15] of 250 t C ha^{-1}, and taking into account that 50% of the PSF trees remained standing after fire, we estimate this to be 0.05 Gt for the 2.5-Mha study area. The biomass produced on bushland, agricultural and plantation areas, collectively, is negligible compared to that on the various forest cover types and has been ignored.

It is almost impossible to determine, with precision, the total area of landscape in Indonesia that burned in the 1997 fires, or how much of that was peatland, because data are few, conflicting and vary enormously. A report by the Indonesian Development Planning Agency, for example, provides a range from 0.16 to 9.50 Mha for the whole of Indonesia[9], while studies[10,14] using low-resolution satellite imagery suggest that 3–13 Mha were affected in Kalimantan and Sumatra alone. None of these studies identified the area of peatland that was affected. The estimate of 1.45 Mha of peatland burned in the whole of Indonesia during 1997[9] includes data for Sumatra (300,000 ha), Kalimantan (750,000 ha) and West Papua (400,000 ha) and provides a value of 0.48–0.56 Gt for carbon loss. We believe this to be an underestimate, because of (1) the inaccuracy of the methods used to determine the areas of different land cover types burned, (2) the lack of detailed satellite and ground truth information to differentiate between areas of peatland versus non-peatland that burned, and (3) the use of data for forested peatland only, whereas agricultural land on peat is excluded.

By applying our values of an average of 0.51 ± 0.05 m of peat burned away over 33.9% of the peat-covered landscape of Central Kalimantan to the 20.07 Mha of peatland in Indonesia[4], and assuming that 50% of above-ground biomass (at 250 t C ha^{-1}) was burned, we estimate that between 2.18 and 2.57 Gt of carbon could have been released to the atmosphere from these catastrophic fires. We also provide an intermediate scenario, based on a fire-damaged peatland area of 2.44 Mha (derived from a combination of verifiable and uncorroborated sources) of a release of 0.81–0.95 Gt C. This is also likely to be an underestimate, because the information for Sumatra has not been acquired with the same degree of stringency as that for Kalimantan, and there are no reliable data for West Papua. We conclude that the most likely amount of carbon released from burning of peat and its surface vegetation in Indonesia was between 0.81 and 2.57 Gt. This is 13–40% of the current global annual carbon emissions from the burning of fossil fuels (6.4 Gt C yr^{-1}), and would have been a major contributor to the sharp increase in atmospheric CO_2 concentrations detected in 1998—from the 1990–99 average of 3.2 ± 0.1 Gt C yr^{-1} to 6.0 Gt C yr^{-1}, the highest value recorded since direct measurements began in 1957[1].

The extensive fire damage caused in 1997 has accelerated changes already being caused in tropical peatlands by forest clearance and drainage. We found, by assessing logging activity in Landsat images for our 2.5-Mha study area for 1997 and 2000, that logging had increased by 44% during this period, thus making the remaining forests more susceptible to fire in the future. This is a matter of concern because natural, undamaged PSF is essential to maintain high water levels, protect the peat carbon store and facilitate future carbon sequestration from the atmosphere. If more PSF is destroyed by logging, development and fire, there will be a continued release of carbon through decomposition of the exposed peat surfaces that, in turn, will place this large carbon store at further risk. Tropical peatlands will make a significant contribution to global carbon emissions for some time to come unless major mitigation, restoration and rehabilitation programmes are undertaken. □

Methods

Satellite image processing and interpretation

Pre-fire land cover and the area burned were obtained from two Landsat TM images, one from shortly before the fires commenced in 1997 (Landsat TM 5, 118-62, 29 May 1997) and the other after the end of the fires (Landsat TM 5, 118-62, 29 March 1998). The two images were spectrally adjusted to each other by histogram matching, then contrast-enhanced, co-registered using a set of 24 ground control points, and geo-referenced using 36 Global Positioning System (GPS) measured ground control points. Interpretation of Landsat TM images (channels 1–5) was carried out by visual on-screen digitizing at a scale of 1:100,000 (minimal mapping unit 50 ha). The interpretation key for land cover and burned surfaces was established from GPS ground measurements. The land cover legend was adapted from the TREES classification scheme[13]. Logging activity was determined from two Landsat ETM images (118-62, 29 May 1997 and 12 August 2000) by visual image interpretation. Difference detection techniques[16] to map the burned areas were applied to pairs of ERS SAR images acquired by the high resolution Active Microwave Instrument (AMI, 25-m ground resolution). This instrument detects structural features of the Earth's surface (volume scattering) and the moisture content of the vegetation (dielectric properties)[17]. Fire decreases both. Volume scattering decreases because fire consumes vegetation and moisture content decreases because fire-damaged plants lose their foliage. Furthermore, the opened canopy and the reduced leaf biomass allow more backscatter from the exposed ground surface. A mosaic of 6 ERS images was made out of 12 ERS images (frame nos 3645, 3663; orbits 07873, 11652, 12110, 12883, 13112, 32828) acquired before the fires (beginning of July 1997) and towards the end of the fire season (October 1997). Images acquired after rain had started again (November 1997) were not suitable for evaluation because surface water in swamps disturbed burn scar detection.

Pre- and post-fire images were co-registered to form bi-temporal image pairs. Co-registration was done automatically using the SAR Toolbox (ESA) with a registration error of less than one pixel. The images were calibrated to represent radar image backscatter, sub-sampled to 25 m pixel size, speckle filtered, and georeferenced (using orbital information and 36 GPS measured ground control points). The bi-temporal mosaic was visually interpreted on-screen (scale 1:200,000, minimal mapping unit 100 ha). The interpretation of SAR signatures was based on GPS-mapped ground observations and evaluation of 42 digital video sequences. Fire occurrence was confirmed using coarse resolution images from the Advanced Very High Resolution Radiometer (AVHRR, 1,100-m ground resolution) onboard the NOAA 12 and 14 satellites, which were processed to detect hot spots by the IFFM fire monitoring centre in Samarinda, East Kalimantan. During a period of 338 d from January 1997 to December 1997, 15,908 hot spots were recorded in the study area. An area was acknowledged as burned only when there was either clear decrease in backscatter, or weak decrease in backscatter in conjunction with NOAA-AVHRR hotspot evidence. Quantitative analysis and intersection of the resulting thematic maps were carried out in a Geographical Information System. The area was confined to the overlapping region in all remote sensing data sets (25,000 km^2).

Ground surveys and field measurements

Since 1993, we have been carrying out large-scale ecological field research on PSF in Central Kalimantan, during which we have acquired an extensive database of information on tropical peatland biodiversity and natural resource functions. This ecosystem is almost inaccessible because it is flooded for up to 10 months of the year, the ground surface is very uneven, the vegetation is virtually impenetrable and there are several health and safety concerns. For this study, extensive ground-truthing, involving travel of over 3,000 km, had been carried out before the fires in order to check image classification of land-use and vegetation within the study area. Post-fire ground-truthing to verify the existence and magnitude of land cover types and burn scars was made at 145 GPS-recorded locations (Fig. 1b) and using 4 h of GPS synchronized video material acquired during two aerial surveys (conducted in 1998 and 1999) to check areas that could not be accessed on foot. Classification accuracy for discrimination of burned and unburned surfaces was >95%, based on 184 randomly selected digital video images.

Peat thickness was measured using a manually operated peat corer; we found that the PSF is very dense, and that trees are preserved within the peat mass. The surface levels of the peat-covered landscape relative to the adjacent main rivers, and the thickness of the underlying peat, were determined at 126 locations at intervals of 500 m along the main channels in Block C of the MRP. These channels were the only way to gain access to otherwise impenetrable burned and unburned PSF, and they enabled data to be collected on a grid basis at several locations both across and along the watershed. This peat inventory involved 6 people for a period of 4 months in 1999/2000. Peat volume was calculated from the peat area occupied by different land cover types, determined by satellite imagery, and GIS IDW interpolation of peat thickness, obtained from the field drilling. The IDW average was found to be adequate because all of the peatlands investigated in this study were dome-shaped and thus did not show extreme values. For the

IDW interpolation we set all boundary values to a minimum peat thickness of 50 cm. For the calculation we used cell size 100 m, nearest neighbour, power 2 and no barriers. For loss of peat thickness as a result of the fires, we made 43 measurements in several locations in mixed swamp forest in block C of the MRP, at a distance of about 7 km from the edge of the peat dome and more than 0.5 km from the nearest drainage channel.

Received 20 March; accepted 17 September 2002; doi:10.1038/nature01131.

1. Houghton J. T. *et al. Climate Change 2001: The Scientific Basis* (ed. Houghton, J. T.) (Cambridge Univ. Press, Cambridge, 2001).
2. Page, S. E. & Rieley, J. O. Tropical peatlands: a review of their natural resource functions with particular reference to Southeast Asia. *Int. Peat J.* **8,** 95–106 (1998).
3. Sorensen, K. W. Indonesian peat swamp forests and their role as a carbon sink. *Chemosphere* **27,** 1065–1082 (1993).
4. Rieley, J. O., Ahmad-Shah, A. A. & Brady, M. A. *Tropical Lowland Peatlands of Southeast Asia* (eds Maltby, E., Immirzi, C. P. & Safford, R. J.) 17–53 (IUCN, Gland, Switzerland, 1996).
5. Page, S. E., Rieley, J. O., Shotyk, W. & Weiss, D. Interdependence of peat and vegetation in a tropical peat swamp forest. *Proc. R. Soc. Lond. B* **354,** 1–13 (1999).
6. Watson R. T. *et al. Land Use, Land Use Change and Forestry* (ed. Watson, R. T.) (Cambridge Univ. Press, Cambridge, 2000).
7. Barber, C. V. & Schweithelm, J. *Trial by Fire – Forest Fires and Forestry Policy in Indonesia's Era of Crisis and Reform* (World Resources Institute, Washington DC, 2000).
8. Siegert, F., Rücker, G., Hinrichs, A. & Hoffmann, A. Increased fire impacts in logged over forests during El Niño driven fires. *Nature* **414,** 437–440 (2001).
9. ADB (Asian Development Bank)/BAPPENAS (National Development Planning Agency) *Causes, Extent, Impact and Costs of 1997/98 Fires and Drought* Final Report, Annex 1 and 2, *Planning for Fire Prevention and Drought Management Project* (Asian Development Bank TA 2999-INO Fortech, Pusat Pengembangan Agribisnis, Margueles Pöyry, Jakarta, Indonesia, 1999).
10. Fuller, D. O. & Fulk, M. Burned area in Kalimantan, Indonesia mapped with NOAA-AVHRR and Landsat TM imagery. *Int. J. Remote Sens.* **22,** 691–697 (2001).
11. Bowen, M. R., Bompard, J. M., Anderson, I. P., Guizol, P. & Gouyon, A. *Forest Fires and Regional Haze in Southeast Asia* (eds Eaton, P. & Radojevic, M.) 52–66 (Nova Science, New York, 2000).
12. Bompard, J. M. & Guizol, P. *Land Management in South Sumatra Province, Indonesia. Fanning the Flames: the Institutional Cause of Vegetation Fires* (European Union Forest Fire Prevention and Control Project and Indonesian Ministry of Forestry and Estate Crops, Jakarta, 1999).
13. Stiebig, H.-J., Achard, F., Eva, H., Mayaux, P. & Richards, T. *Forest Cover Change Assessment at the Pan-Tropical Scale using Earth Observation Satellite Data* (IUFRO, Kuala Lumpur, 2000).
14. Liew, S. C., Lim, O. K., Kwoh, L. K. & Lim, H. *Proc. 1998 Int. Geoscience and Remote Sensing Symp.* 879–881 (IEEE, Piscataway, New Jersey, 1998).
15. Jordan, C. F. *Tropical Rain Forest Ecosystems. Ecosystems of the World 14* (ed. Golley, F. B.) 117–135 (Elsevier, Amsterdam, 1983).
16. Siegert, F. & Rücker, G. Use of multitemporal ERS-2 SAR images for identification of burned scars in Southeast Asian tropical rain forest. *Int. J. Remote Sens.* **21,** 831–837 (2000).
17. Ulaby, F. T., Moore, R. K. & Fung, A. K. *Microwave Remote Sensing: Active and Passive Vol III, From Theory to Applications* 1811–1830 (Artech House, Dedham, 1986).
18. Neuzil, S. G. *Biodiversity and Sustainability of Tropical Peatlands* (eds Rieley, J. O. & Page, S. E.) 55–72 (Samara, Cardigan, UK, 1997).

Acknowledgements NOAA AVHRR hotspot data were provided by the IFFM/GTZ Integrated Forest Fire Management Project. This work was supported by the European Union and the UK Darwin initiative.

Competing interests statement The authors declare that they have no competing financial interests.

Correspondence and requests for materials should be addressed to S.E.P. (e-mail: sep5@le.ac.uk).

The origin of geomagnetic jerks

Jeremy Bloxham*, Stephen Zatman†‡ & Mathieu Dumberry*

* *Department of Earth and Planetary Sciences, Harvard University, Cambridge, Massachusetts 02138, USA*
† *Department of Earth and Planetary Sciences, Washington University, St Louis, Missouri 63130, USA*
‡ *Deceased*

Geomagnetic jerks, which in the second half of the twentieth century occurred in 1969 (refs 1, 2), 1978 (refs 3, 4), 1991 (ref. 5) and 1999 (ref. 6), are abrupt changes in the second time-derivative (secular acceleration) of the Earth's magnetic field. Jerks separate periods of almost steady secular acceleration, so that the first time-derivative (secular variation) appears as a series of straight-line segments separated by geomagnetic jerks. The fact that they represent a reorganization of the secular variation implies that they are of internal origin (as has been established through spherical harmonic analysis[7]), and their short timescale implies that they are due to a change in the fluid flow at the surface of the Earth's core (as has also been established through mapping the time-varying flow at the core surface[8]). However, little is understood of their physical origin. Here we show that geomagnetic jerks can be explained by the combination of a steady flow and a simple time-varying, axisymmetric, equatorially symmetric, toroidal zonal flow. Such a flow is consistent with torsional oscillations in the Earth's core, which are simple oscillatory flows in the core that are expected on theoretical grounds[9], and observed in both core flow models[10] and numerical dynamo models[11].

In Fig. 1 we show the secular variation of the magnetic field at Niemegk (Germany) and Macquarie Island (Australia) observatories for the period 1950–2001. At Niemegk, the secular variation of the Y (east) component is simply described: it is linearly decreasing until around 1969, then linearly increasing until 1978, linearly decreasing to 1990, and linearly increasing to 1999. Although the abrupt nature of the geomagnetic jerks which mark the transitions between these intervals of nearly linear secular variation at 1969, 1978, 1991 and 1999 has been the focus of most attention, the near linear trend of the secular variation between the jerks is also noteworthy; for a review see ref. 12. However, at Macquarie Island (which is roughly antipodal to Niemegk) the secular variation is much less straightforwardly characterized, with little or no evidence of magnetic jerks.

The fact that jerks are most readily observed at European observatories, are largely confined to one component of the field, and are abrupt, argues for a local origin, perhaps a magnetic field instability. Arguing against such an origin is the fact that they represent transitions between long intervals of linear secular variation; in other words, jerks are not simply transient perturbations to the secular variation, instead they delineate intervals of oppositely signed secular acceleration.

The most powerful tool that we have available for investigating the origin of the secular variation is the frozen-flux hypothesis[13], which states that on timescales short compared to that of magnetic diffusion the secular variation results primarily from the rearrangement of the magnetic field by fluid flow at the core surface. We find that a substantial portion of the secular variation over the past 150 years can be explained with a steady fluid flow[14]. Nonetheless, significant signal remains unexplained, including geomagnetic jerks. Here we explore whether the remaining signal can be explained with a simple, physically plausible, time-varying flow.

To a first approximation, the geomagnetic dynamo is expected to operate in a Taylor state[9], where the magnetic field in the core is arranged so that the axial Lorentz torque vanishes when integrated over the surface of cylinders coaxial with the rotation axis. Small departures from this state would cause angular accelerations of these cylinders about the Earth's rotation axis, resulting in torsional oscillations, which are oscillatory differential rotations of these cylinders. Representing this flow at the core–mantle boundary using vector spherical harmonics[15], we have

$$\mathbf{u}_T(s,t) = \nabla \times (T(s,t)\hat{\mathbf{r}}) \tag{1}$$

where $\mathbf{u}_T$ is the fluid flow, s is distance from the rotation axis, $\hat{\mathbf{r}}$ is a unit vector in the radial direction and t is time, with

$$T(s,t) = \sum_{l \text{ odd}} T_l(t) P_l^0(\cos\theta) \tag{2}$$

where θ is colatitude. This is an extremely parsimonious representation of the time-dependent part of the flow: for a flow up to spherical harmonic degree n, only $n/2$ out of the $2n^2 + 4n$ spherical harmonic coefficients of the flow are included. It is important to note that this work is distinguished from previous attempts to explain geomagnetic jerks with time-varying flow[16–18] by the fact